DEPENDENCE OF AE PARAMETERS ON THE PROPAGATION DISTANCE

D. POLYZOS[1], A. PAPACHARALAMPOPOULOS[1], T. SHIOTANI[3] and D. G. AGGELIS[4]

[1] Department of Mechanical Engineering and Aeronautics, University of Patras, Rio 26500, Greece. [2] Graduate School of Engineering, Kyoto University, Kyoto 615-8540, Japan. [3] Department of Material Science and Engineering, University of Ioannina, Ioannina, 45110, Greece.

Abstract

Acoustic emission (AE) technique is used to monitor the fracture process in engineering materials and structures. The pulse emitted during a cracking incidence depends on the motion of the crack tip and supplies information on the mode of active cracking. Therefore, AE data are used for classification of the dominant cracking mode. This is significant since nucleation of shear cracks generally follows tensile ones on an existing failure surface and crack characterization gives insight in the current stage of the fracture process. The differences in the microscopic motion of the crack sides for the distinct crack modes results in noticeable changes in the AE signals, concerning their shape and frequency content. However, due to inherent inhomogeneity of the materials the pulse is strongly distorted until reaching the AE sensor on the surface. This effect is accumulated with propagation distance and renders crack classification troublesome for large structures. In the present study, the Boundary Element Method (BEM) is employed and numerical simulations dealing with the propagation of AE signals generated by the loading of straight and inclined surface breaking cracks are conducted. This study includes both the generation of the pulse from a crack propagation incidence of a surface breaking crack and reception of the corresponding wave at several different positions. The relative motion of the crack sides is varied in order to simulate different crack modes, while different crack tip geometries are investigated. Waveform analysis reveals the strong dependence of AE parameters on the distance between the source crack and the receiving point, stressing out that the influence of distance is crucial and should be taken into account for successful cracking mode characterization.

Introduction

Acoustic emission (AE) is a method widely used for real time monitoring of the structural condition of different materials and structures. It is based on the elastic energy, which is released after each crack propagation incidence. This energy is transmitted through the material in the form of elastic waves and can be detected by appropriate sensors on the surface of the material [1]. The accumulated activity recorded by the sensors is indicative of the severity of cracking, since the existence of cracks is usually the prerequisite for AE generation. Certain indices based on the magnitude or the number of the AE signals has been employed successfully in the health monitoring of heterogeneous structural materials like concrete and composites [2-4]. When multiple sensors are applied, apart from the number of AE hits, significant information concerning the location of the source events can be derived based on the time delay between acquisition of the corresponding signals at different sensors [5]. This allows estimation of which part of the material needs repair, which is of paramount importance for large-scale structures.

However, there are other important aspects of the AE testing, which are based on the qualitative parameters of the received signals. It has been seen that the shape of the waveforms is indicative of the fracture type, something very important for the classification of cracks in different

materials [6-9]. Shear cracks follow tensile cracks as damage is being accumulated within the material. Therefore, the characterization of the cracking mode can act as a warning against final failure. It has been shown that tensile events are linked to higher frequency content and higher RA value (rise time/amplitude, μs/V; see Fig. 1) than shear [7, 8, 10]. This kind of classification has proven useful in laboratory conditions concerning corrosion cracking in concrete [7], fracture of cross-ply laminates [6, 9, 11], as well as discrimination between tensile matrix cracking and fiber pull-out during bending of steel-fiber reinforced concrete [12]. However, it should be kept in mind that the AE signals are elastic waves, which are scattered while propagating from the source to the sensors. The shape of the waveform will change depending on the heterogeneity of the path, either due to the constituent phases if a composite material is examined or/and due to the existence of cracks [13, 14]. Since the shape of the wave changes, it is expected that the calculation of AE parameters will be affected. This practically means that one specific event will be recorded as having different waveform shapes for sensors placed at close or further distances from the source. Therefore, the influence of the distance in the measurement of AE parameters should be studied especially in relation with standardization, which is currently being attempted for the field of concrete [10, 15].

In the present paper, the relation between the measured AE parameters and the fracture mode and propagation distance through a concrete-like elastic medium is numerically studied. Simulations are used to examine the waveform shape change due to the simultaneous propagation of distinct wave modes with different velocities on the surface. The transient waveforms are recorded at different locations to simulate different AE sensors on the surface of the material.

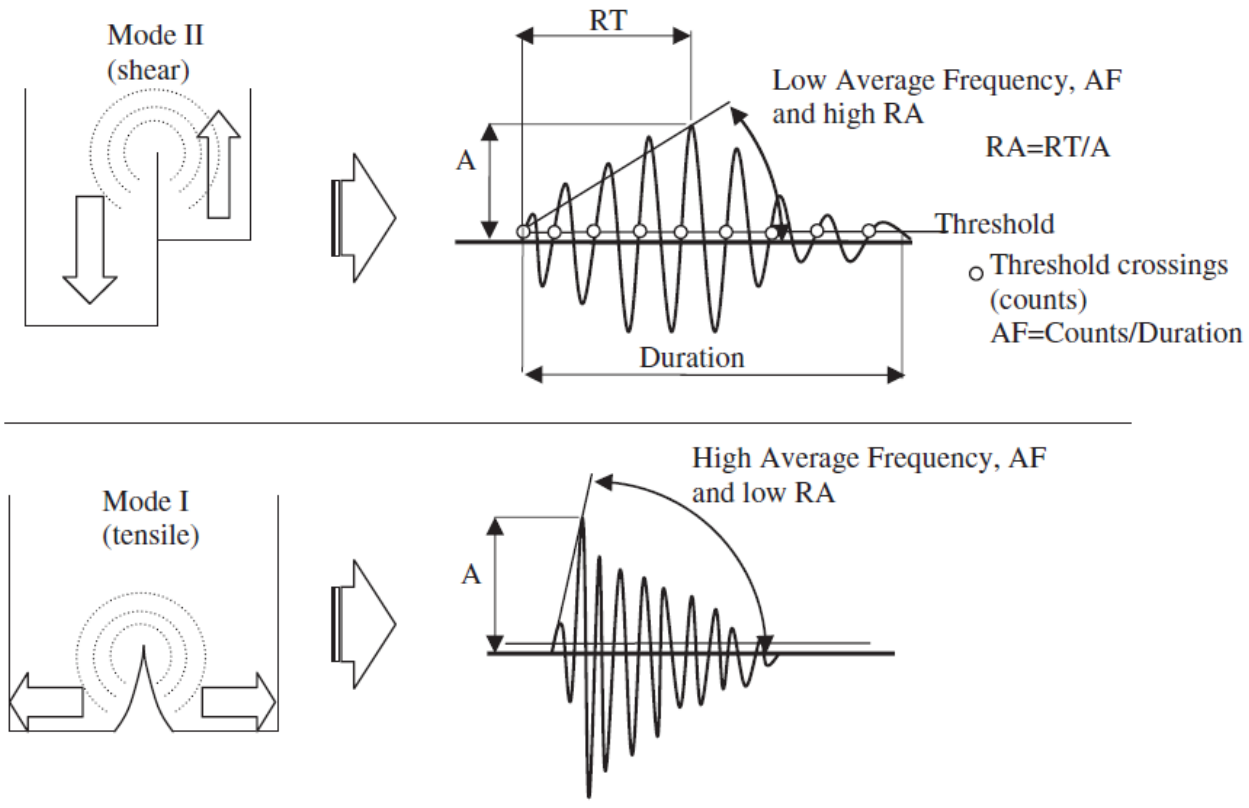

Fig. 1. Schematic view of RA and average frequency, AF.

Numerical Simulation of AE Signals via BEM

In the present section the boundary element method (BEM) is exploited for the numerical simulation of AE signals created by straight and inclined surface breaking cracks subjected to Mode I & II loading.

Consider a two-dimensional linear elastic half-space of surface S and a straight or inclined surface breaking crack subjected to Mode I or Mode II loading as shown in Fig. 2. The excitation of the tip of the crack through a suddenly applied displacement field creates AE pulses captured by equally spaced transducers located on the free surface of the considered concrete space, also depicted in Fig. 2. Applying fast Fourier transform (FFT) on the excitation signal, the above time domain problem is decomposed to a sequence of harmonic boundary value problems that can be solved with the aid of the BEM.

For each frequency ω the corresponding displacement vector $\mathbf{u}$ satisfies the Navier–Cauchy differential equation:

$$\mu\nabla^2\mathbf{u}+(\lambda+\mu)\nabla\nabla\cdot\mathbf{u}+\rho\omega^2\mathbf{u}=\mathbf{0} \tag{1}$$

where λ,μ and ρ stand for the Lamé constants and the mass density, respectively, ∇,∇^2 represent the gradient and Laplace operator, respectively and ω the excitation angular frequency. Considering the fundamental displacement tensor $\mathbf{u}^*$ and the corresponding fundamental traction $\mathbf{t}^*$ of the above differential equation and employing Betti's reciprocal identity, one can obtain the integral representation of the harmonic problem in the form [16]:

$$\frac{1}{2}\mathbf{u}(\mathbf{x})+\int_S \mathbf{t}^*(\mathbf{x},\mathbf{y},\omega)\cdot\mathbf{u}(\mathbf{y})dS_\mathbf{y}=\int_S \mathbf{u}^*(\mathbf{x},\mathbf{y},\omega)\cdot\mathbf{t}(\mathbf{y},\omega)dS_\mathbf{y} \tag{2}$$

For the present problem where both the surface of the crack and the surface of the half space are traction free, i.e. $\mathbf{t}(\mathbf{y},\omega)=\mathbf{0}$ the integral equation (2) is written as

$$\frac{1}{2}\mathbf{u}(\mathbf{x})+\int_{S+S_1} \mathbf{t}^*(\mathbf{x},\mathbf{y},\omega)\cdot\mathbf{u}(\mathbf{y})dS_\mathbf{y}=\int_{S_2} \mathbf{t}^*(\mathbf{x},\mathbf{y},\omega)\cdot\mathbf{U}(\mathbf{y},\omega)dS_\mathbf{y} \tag{3}$$

with $\mathbf{x}$ being the point where the corresponding displacement vector $\mathbf{u}$ is evaluated, $\mathbf{U}$ is the excitation displacement vector corresponding to frequency ω, S is the free surface of the half space, S_1 the traction-free surface of the crack and S_2 the tip of the crack where $\mathbf{U}$ is imposed.

Integral equation (3) is solved numerically by discretizing S, S_1, S_2 into continuous, isoparametric, quadratic line elements, while a combination of continuous–discontinuous or partially discontinuous elements is used for corners and discontinuous boundary conditions. The truncation of the free surface is accomplished by considering that the reflected Rayleigh waves do not affect the transient signal at the observation point [17]. Collocating the discretized integral Eq. (3) at each node, one obtains a system of linear algebraic equations having the form

$$[\mathbf{H}]\cdot\{\mathbf{u}\}=\{\mathbf{b}\} \tag{4}$$

where vector $\{\mathbf{b}\}$ contains all the known displacements of the excited nodes of surface S_2, $\{\mathbf{u}\}$ is a vector with all the unknown displacements at S, S_1 and [H] is a matrix comprising regular, weakly singular and hypersingular integrals all numerically evaluated through advanced integration techniques explained in [16]. The linear algebraic system (4) is solved numerically through a LU decomposition algorithm and the evaluated displacements are converted to time domain through the inverse FFT procedure.

In order to minimize the aliasing phenomena, the exponential window method proposed by Kausel and Röesset [18] is utilized, where complex frequencies with a small imaginary part of the form: $\omega_c = \omega - jc$ are used. The constant c is set equal to $0.65\Delta\omega$ where $\Delta\omega$ is the frequency step used in FFT. After numerically solving the problem in the frequency domain and then applying the inverse Fourier transform, the time response is rescaled with the aid of the exponential factor e^{ct}.

Figure 2 depicts the basic geometry including the surface breaking crack and the recording transducers. The simulation of Modes I and II was accomplished by accordingly changing the direction of the applied displacement field on the crack tip. Two different types of excitation waveforms were used, namely short (1 cycle) and long (20 cycles). The basic excitation frequency was 150 kHz. The case of slightly curved crack tips was also considered in order to explore the effect of crack geometry on the received signals. The specific material properties were λ = 11 GPa, μ = 17 GPa and ρ = 2.3 Mg/m^3, resulting in a longitudinal wave velocity of 4735 m/s.

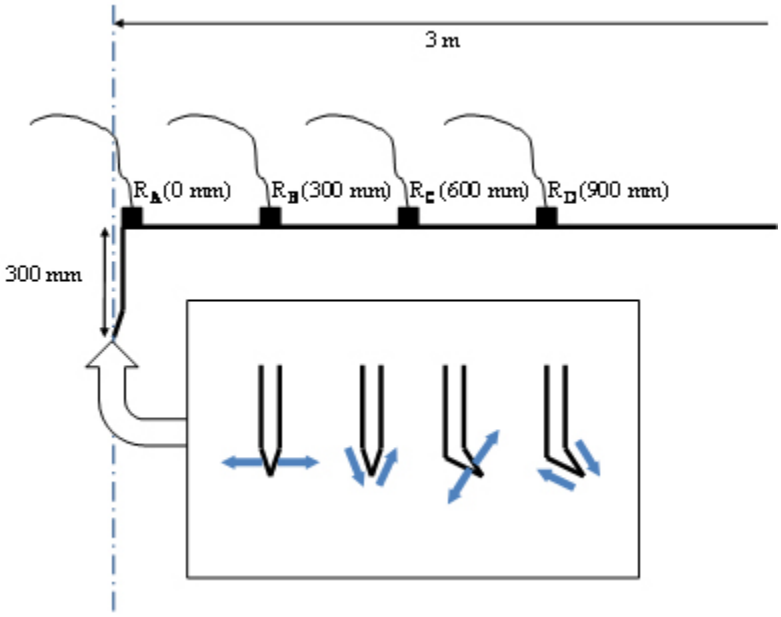

Fig. 2 Geometry of the problem solved via BEM.

Results

Influence on Waveform Shape

Two types of pulses were used for excitation: short (one cycle) and long (several cycles). The short pulse enables the separation of the different wave modes after propagation. This helps one understand wave propagation and identification of different modes and reflections that would not be possible for a long-pulse excitation. On the other hand, experimental AE signals are quite long, as also influenced by the resonance behavior of AE sensors, which limit the bandwidth, causing an increase in time domain duration. Before the main analysis of the long realistic signals is presented and analyzed, it is essential to discuss some qualitative aspects of propagation, which are clearer for the short pulse.

Figure 3a shows the waveforms captured by the four receivers after Mode I short pulse excitation on the curved crack geometry. These waveforms stand for the vertical motion of the surface nodes that correspond to each "receiver". The initial weak burst belongs to the longitudinal

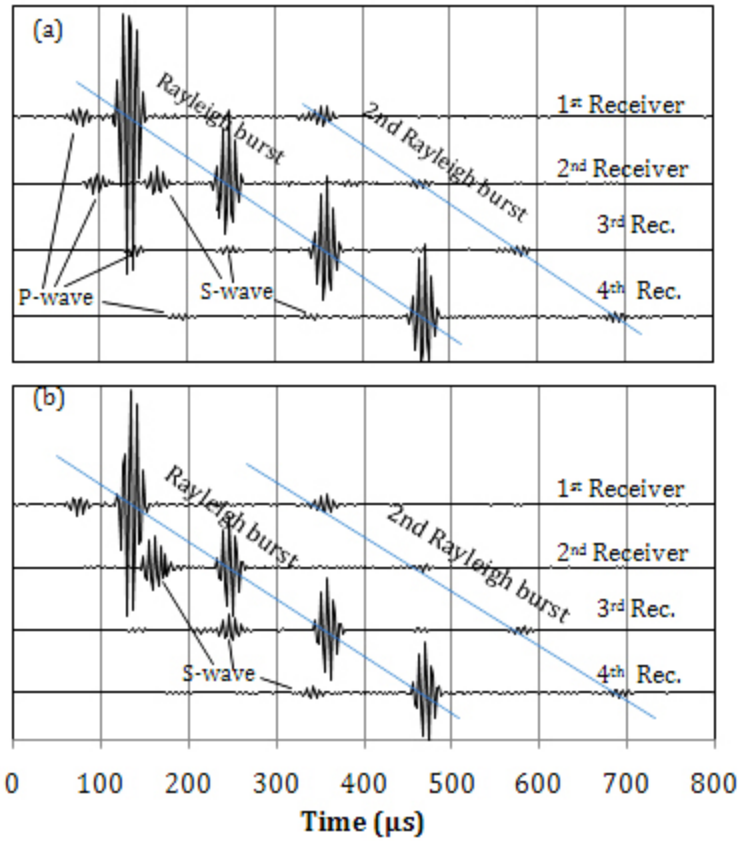

Fig. 3 Waveforms for the four receiver points after short pulse (a) mode I excitation, (b) mode II excitation in the inclined crack.

(P-) wave, which is the fastest mode and can be seen in all four waveforms. Focusing on the waveform of the first receiver, a stronger burst is obtained after 100 μs, corresponding to the Rayleigh wave that contains most of the energy after excitation. Until reaching the 1st receiver, all different wave modes travel along the crack side. A part of the energy is reflected from the surface back to the crack tip while another continues on the horizontal surface line. Therefore, the Rayleigh burst can be easily identified at the successive receivers after equal intervals of 110 μs, which is the transit time needed for the Rayleigh wave to propagate the distance of 300 mm between receivers. Another Rayleigh burst can be identified, approximately 220 μs after the first in all waveforms (Fig. 3a), due to reflection from the surface to the tip and back reflection from the tip to the surface. The 2nd Rayleigh burst is considerably weaker since in each reflection point a part of energy is converted to P- and S- wave modes. Rayleigh waves can be identified even after long propagation because of negligible spreading, since in the two-dimensional space, Rayleigh waves are limited to the surface of the material. On the other hand, P-wave suffers spreading even in two-dimensions and therefore, it can be identified only by the initial propagation and not after possible reflections. The shear wave is located between the P- and R- components for all receivers, except for the 1st, where it has still not separated from the Rayleigh, which travels at almost the same speed. On the other receivers, the S- components are well separated mainly because they travel to the receivers on a straight line, while the Rayleigh has to traverse the crack side until reaching the top surface and thus covers more distance before being felt by receivers 2 to 4. This is the reason why the delays between the Rayleigh burst at successive receivers are equal, while this is not the case for P- and S- waves.

Figure 3b shows the corresponding waveforms at the exactly same geometry (inclined crack) after shear (Mode II) excitation. The main features of the waveforms are similar to the previous case, with the main wave components recorded at the same intervals. It is seen, therefore, that in the event of a surface crack, most of the energy propagates in the form of Rayleigh waves. The mode of the source excitation seems to have only slight qualitative effect on the received waveform. However, one distinct difference between the waveforms collected after Mode I or II excitation is the proportion between P- and S- waves. In the second case (Fig. 3b, Mode II) the shear component is apparently stronger than the P-wave, which is negligible after the 2nd receiver. This shows that according to the mode of excitation the energy is reasonably translated to different modes and as a result of the different wave speeds, the shape of the acquired waveform is expected to differ.

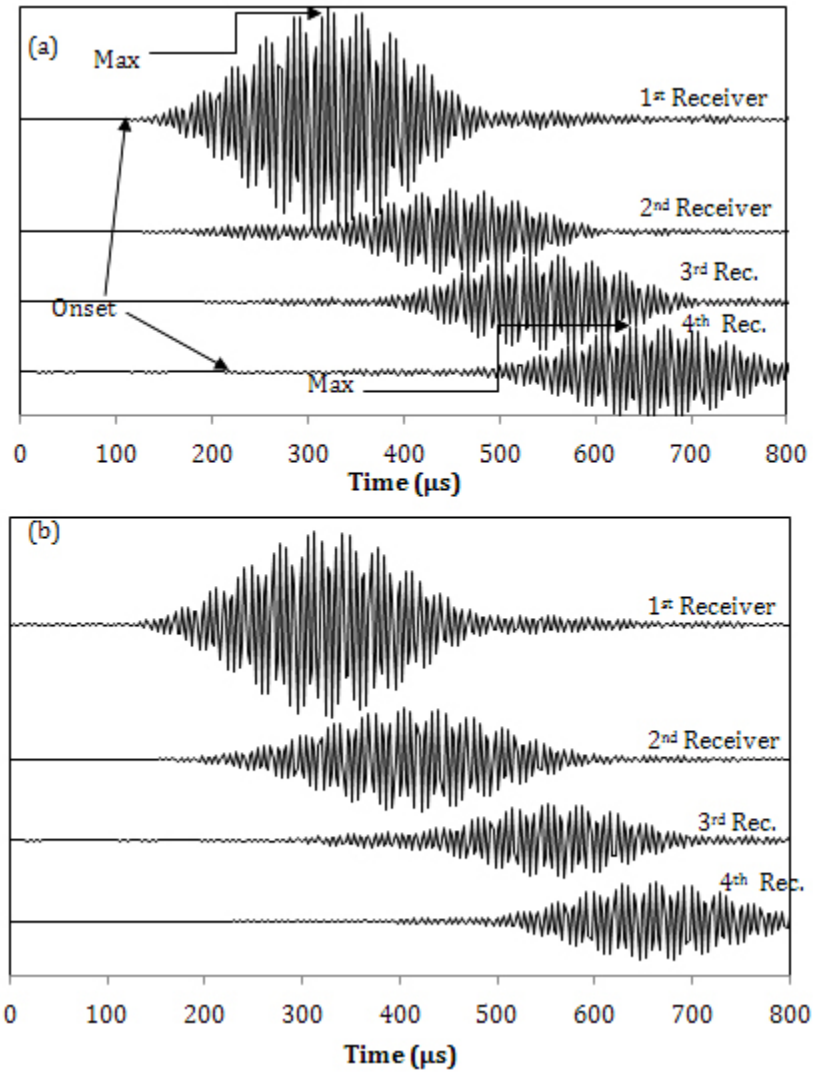

Fig. 4 Waveforms for the four receiver points after long pulse (a) Mode I excitation, (b) Mode II excitation in the inclined crack.

In order to produce realistic results and measure AE parameters as commonly done in AE practice, longer pulse excitation was applied. The excitation consisted of 10 cycles of 150 kHz in a sinusoidal envelope, in order to resemble the resonance frequency of commercially used transducers [8, 12], while other central frequencies are also applicable. The waveforms for Mode I and II excitations are seen in Fig. 4a and 4b respectively for the geometry of the inclined crack.

Seemingly there are no strong differences between the two modes. As a general comment, the different wave types are not separated and the waveform is a long burst of several cycles. One of the visible differences as the distance from the crack increases, is that the main energy of the wave envelope is translated backwards compared to the onset of the pulse (see Fig. 4a). This is mainly due to the Rayleigh component that arrives later compared to the initial P-wave and thus the calculated AE parameters shall differ considerably. In order to calculate the specific AE parameters the threshold was set equal to 2% of the maximum amplitude of each waveform, while comparisons using threshold of 5% are also conducted.

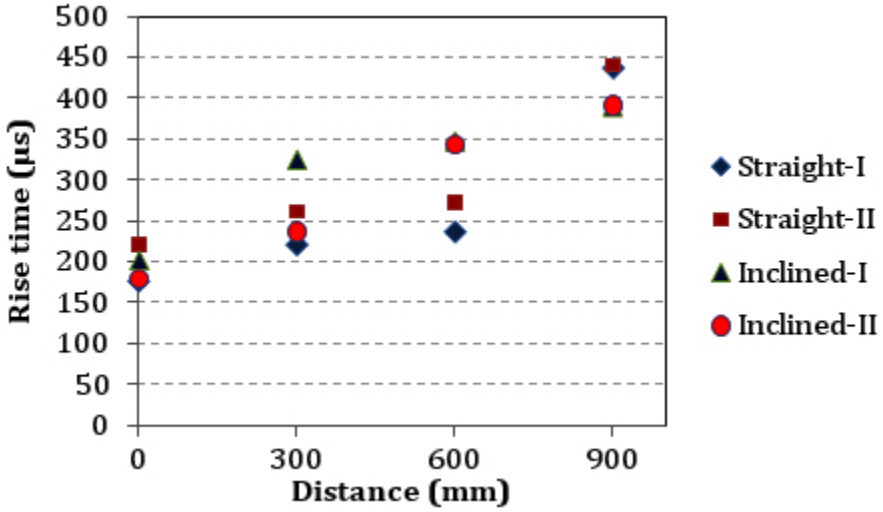

Fig. 5 Rise time vs. horizontal distance from the crack for different crack geometries and excitations and threshold 2% of maximum.

AE Parameters

Figure 5 shows the rise time of the waveforms. For all simulated cases the rise time of the waveform exhibits a steadily increasing trend with distance. RT starts at approximately 200 μs, while for the furthest receiver is calculated at 400-450 μs. This increasing trend is already indicative of the strong dependence of the AE parameters on the propagation distance to the sensors. Since RT is the delay between the time of maximum amplitude and the onset, it is confirmed that the main energy of the waveform is continuously delaying relatively to the weak P-wave component. Figure 6a shows the RA value (RA=RT/A) with respect to distance. In this case there is an also increasing trend vs. distance for all of the simulated cases. Concerning the excitation mode in both geometries (straight and inclined cracks), Mode II results in much higher RA even for the closest receiver. For the nearest receiver on the straight crack geometry, mode I results in RA equal to 33 μs/V, while mode II in 247 μs/V. As the wave propagates to the furthest receiver, RA for Mode II reaches 1500 μs/V while Mode I, although increases, is limited to below 300 μs/V. This is in accordance with and confirms the experimental evidence of several recent studies, where shear cracking induces higher RA than tensile [7, 8, 10-12].

However, the cracking mode is not the unique parameter that influences RA. One other interesting outcome of the simulations that has not been noted before is that the RA values depend also on the geometry of the crack. For Mode I cracking, the straight crack results in RA lower than 300 μs/V even for the furthest sensor, while the curved crack induces higher RA for any sensor up to 1100 μs/V. Similarly, for Mode II, the curved geometry results in RA values of more than 2500 μs/V, while for the straight crack RA does not exceed 1500 μs/V. The above shows that the geometry of the crack is also important and that a slight inclination of the crack

may interfere with the recorded pulse. The significance of this dependence to distance is that RA values of different mode waveforms overlap; as an example a shear event (Mode II) on the straight crack measured by the closest receiver (horizontal distance of 0 mm) exhibits an RA of 250 μs/V. This is approximately the RA of Mode I excitation on the same geometry measured at the distance of 900 mm. Therefore, a tensile event may be misclassified as shear if the waveform is captured at a long distance from the source. This may well be the case in-situ where long separation distances between sensors are usually applied in order to cover as much volume of the structure as possible with a limited number of sensors. In laboratory, still the influence should not be negligible, since the values of RA change much for 300 mm. In order to check the influence of threshold, Fig. 6(b) shows the RA vs. distance for a different level of threshold, specifically, 5% of the maximum amplitude. Since the threshold is higher, the first few cycles of the waveform may not exhibit threshold crossings. Therefore, RA is in any case lower than the corresponding value measured with lower threshold. This shows that the selection of the threshold should always be taken into consideration because it moderately influences the calculated values. Nevertheless, since contemporary AE equipment can record the whole waveform, analysis with any desired threshold is possible at post-processing stage.

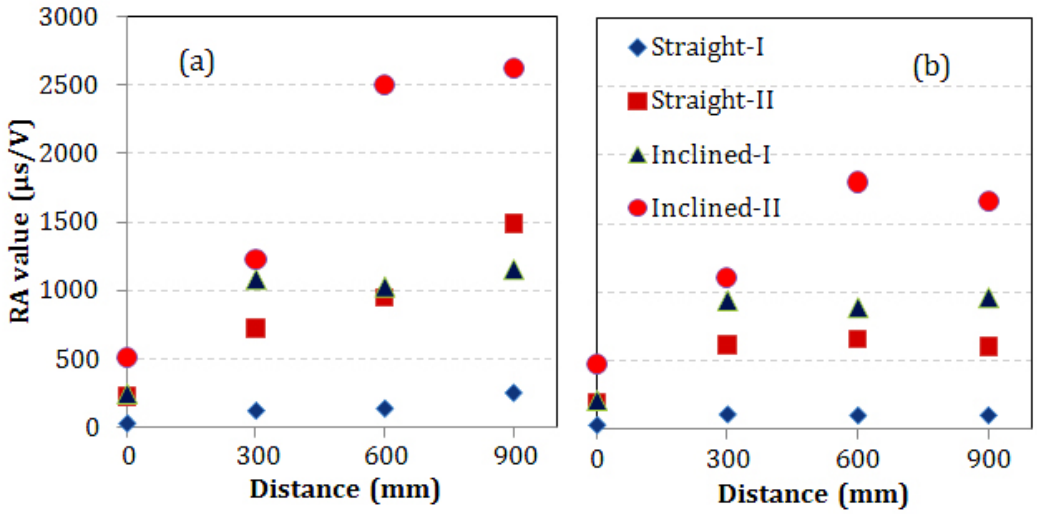

Fig. 6. RA value vs. horizontal distance from the crack for different crack geometries and excitations and threshold (a) 2% of maximum and (b) 5% of maximum amplitude.

In order to evaluate the RA dependence on distance, the results are presented normalized to the RA value of the 1st receiver in Fig. 7. For all simulated cases a strong increase is depicted of the order of 5 to 8 times. This shows that any classification scheme should definitely incorporate the distance information since the measured values that will be used to characterize a cracking event may well differ as measured by adjacent sensors. As an example, it is mentioned that an increase of approximately 4 to 10 times has been measured for the transition between tensile matrix cracking and fiber pull out in steel-fiber reinforced concrete [12], roughly from 500 μs/V to 2000 μs/V. It is reasonable, therefore, that a shift by a factor of 5 or more due to propagation distance would mask the change due to the source crack mode.

Average frequency, AF, is another AE parameter that has been related to the cracking mode. It is calculated as the ratio of the threshold crossings over the duration of the waveform. Figure 8a shows the measured AF values vs. distance. The results do not show any clear trend as a function of distance, the cracking mode or the geometry. In a certain extent, this is reasonable since the geometry corresponds to undamaged material, without any cracks that are strong scatterers of

elastic waves. In case distributed cracks are present in the matrix, the effect of waveform distortion should be more evident and the frequency would be downshifted [19].

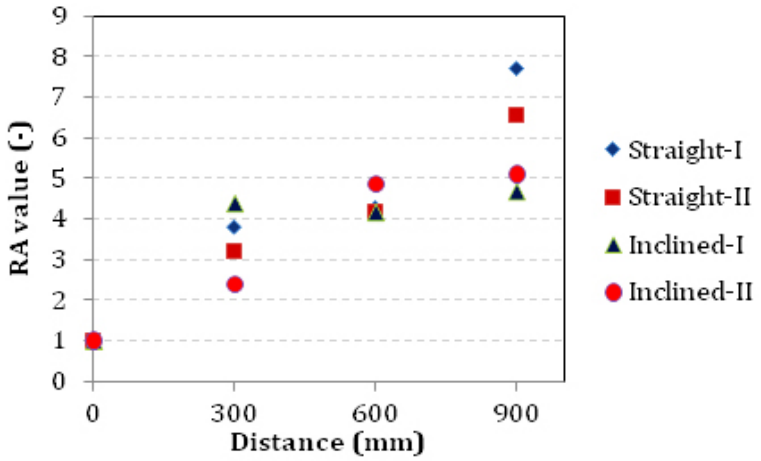

Fig. 7 Normalized RA value vs. horizontal distance from the crack for different crack geometries and excitations at threshold of 2% of maximum.

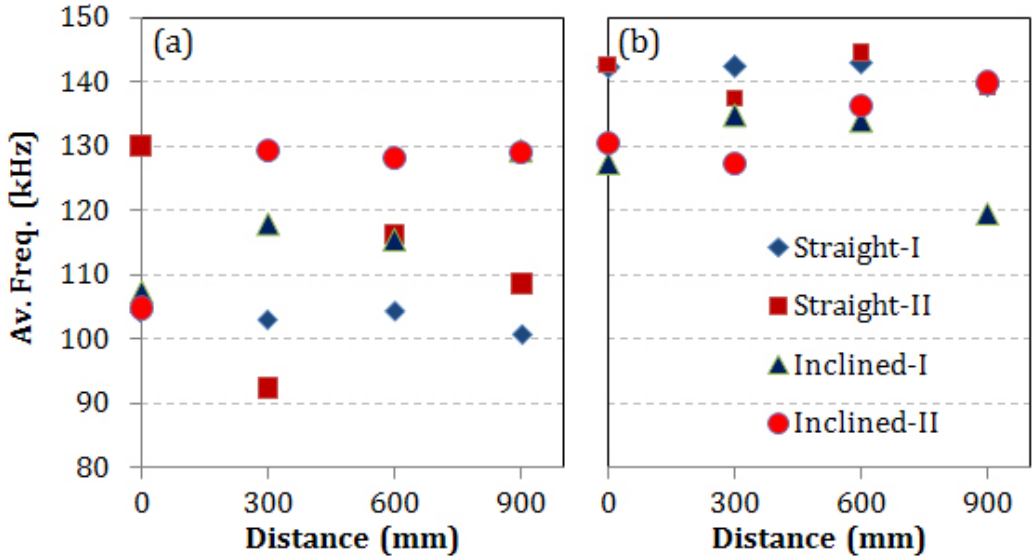

Fig. 8. Average frequency vs. horizontal distance from the crack for different geometries and excitations and threshold (a) 2% and (b) 5% of maximum.

As mentioned earlier, most of the AE parameters are threshold dependent. In order to examine the influence of threshold in the calculation of AF, another threshold of 5% of maximum amplitude was applied. The results are shown in Fig. 8b, again with no specific correlation to distance or mode. The values of AF for the more sensitive lower threshold (2%, Fig. 8a) are slightly lower due to the inclusion of the initial and final weaker parts of the waveform. There, several cycles after the 1st threshold crossing do not cross the threshold and do not "qualify" as crossings (counts), leading to lower frequency measurement. This comparison can be seen in Fig. 6 concerning the RA value. When the higher threshold of 5% is applied, the qualitative conclusions do not change, see Fig. 6b; the values are just translated to lower levels. However, lower and therefore more sensitive threshold is more adequate as it results in wider range of values and stronger discrepancies between the different cases, which allows better characterization. Low ambient noise is crucial therefore in order to allow application of a low and sensitive threshold.

Conclusions

This study presents wave propagation simulations inside an elastic medium after a propagation incidence in a surface-breaking crack. It aims at the better understanding of the effect of different conditions in the calculation of AE parameters. This is important even for small scale applications, since geometry imposes strong influence on the waveforms even for small distances. Consequently, starting from laboratory conditions, and in order to expand the application of AE classification schemes to real structures, the dependence of AE parameters on distance should be further studied. The received signals are compared regarding their original cracking mode (tensile or shear), surface crack geometry (straight or curved), as well as the propagation distance to the sensor, while several other parameters like distributed damage content and microstructure should also be studied in the future. Shear excitation results in higher RA values, as numerous experimental studies suggest. Additionally, the crack geometry seems to strongly influence the shape of the waveforms since higher RA is measured for the curved crack tip, compared to the straight one. The RA value follows an increasing trend with propagation distance, attributed mainly to the lower velocity of Rayleigh waves, which contain most of the energy of the excitation. This increasing trend is strong and should be certainly taken into account in crack classification schemes, since for long distances even "tensile" waveforms would be mistaken as "shear". The importance of a sensitive low threshold is also depicted, while the frequency content does not seem to crucially depend on the distance since the attenuation was not included.

References

[1] Grosse, C. U. and Ohtsu, M. (2008). Acoustic Emission Testing, Springer, Heidelberg.

[2] Kurz, J. H., Finck, F., Grosse, C. U., and Reinhardt, H. W. (2006). "Stress Drop and Stress Redistribution in Concrete Quantified Over Time by the B-Value Analysis," Structural Health Monitoring, **5**: 69-81.

[3] Aggelis, D.G., Shiotani, T., Momoki, S., and Hirama, A. (2009). "Acoustic Emission and Ultrasound for Damage Characterization of Concrete Elements", ACI Materials J., **106**(6): 509-514.

[4] Ono K., Mizutani Y., Takemoto M. (2007). "Analysis of acoustic emission from impact and fracture of CFRP laminates", Journal of Acoustic Emission, **25**, 179-186.

[5] Grosse, C., Reinhardt, H., and Dahm, T. (1997). "Localization and classification of fracture types in concrete with quantitative acoustic emission measurement techniques", NDT&E Int, **30**(4): 223-230.

[6] Anastassopoulos, A.A., and Philippidis, T.P. (1995). "Clustering methodology for evaluation of acoustic emission from composites", Journal of Acoustic Emission, **13**(1/2): 11-22.

[7] Ohtsu, M., and Tomoda, Y. (2007). "Phenomenological model of corrosion process in reinforced concrete identified by acoustic emission", ACI Mater J., **105**(2): 194–200.

[8] Shiotani, T., Ohtsu, M., and Ikeda, K. (2001). "Detection and evaluation of AE waves due to rock deformation", Construction and Building Materials, **15**(5-6): 235-246.

[9] Mizutani Y., Nagashima K., Takemoto M., Ono K. (2000). "Fracture mechanism characterization of cross-ply carbon-fiber composites using acoustic emission analysis", NDT&E International **33**: 101–110.

[10] Ohtsu M. (2010). Recommendation of RILEM TC 212-ACD: acoustic emission and related NDE techniques for crack detection and damage evaluation in concrete, Test method for classification of active cracks in concrete structures by acoustic emission. Materials and Structures, **43**(9): 1187-1189.

[11] Aggelis, D.G., Barkoula, N.M., Matikas, T.E., and Paipetis, A.S. (2010). "Acoustic emission monitoring of degradation of cross ply laminates", Journal of the Acoustical Society of America, **127**(6): EL246-251.
[12] Aggelis, D.G., Soulioti, D.V., Sapouridis, N., Barkoula, N.M., Paipetis, A.S., and Matikas, T.E. (2011). "Acoustic emission characterization of the fracture process in fibre reinforced concrete", Construction and Building Materials, **25**: 4126-4131.
[13] Aggelis, D.G. (2009). "Numerical simulation of wave propagation in material with inhomogeneity: inclusion size effect", NDT&E Int, **42**: 558-563.
[14] Aggelis D. G., Shiotani T., Papacharalampopoulos A., Polyzos D. (2011). "The influence of propagation distance on elastic waves as measured by acoustic emission parameters", Structural Health Monitoring, doi:10.1177/1475921711419992.
[15] RILEM Technical Committee MCM. On-site measurement of concrete and masonry structures by visualized NDT. (http://www.rilem.net/tcDetails.php?tc=MCM).
[16] Polyzos D., Tsinopoulos S. V., Beskos D. E. (1998). "Static and Dynamic Boundary Element Analysis in Incompressible Linear Elasticity", European Journal of Mechanics A/Solids, **17**(3): 515-536.
[17] Kattis S. E., Polyzos D., Beskos D. E. (1999). "Vibration Isolation by a Row of Piles Using a 3-D Frequency Domain BEM", International Journal of Numerical Methods in Engineering, **46**: 713-728.
[18] Kausel E., Röesset J. M. (1992). "Frequency domain analysis of undamped systems", Journal of Engineering Mechanics ASCE, **118**: 721–734.
[19] Aggelis, D. G., and Shiotani, T. (2007). "Experimental study of surface wave propagation in strongly heterogeneous media", Journal of the Acoustical Society of America, **122**(5): EL 151-157.